PERGAMON

Journal of Structural Geology 22 (2000) 683–692

JOURNAL OF STRUCTURAL GEOLOGY

www.elsevier.nl/locate/jstrugeo

Finite-element modelling of simple shear flow in Newtonian and non-Newtonian fluids around a circular rigid particle

Giorgio Pennacchioni[a,*], Luca Fasolo[b], Maria Morandi Cecchi[b], Luca Salasnich[c]

[a]*Dipartimento di Geologia, Paleontologia e Geofisica, Via Giotto 1, CNR—Centro di Studio per la Geodinamica Alpina (CNR—Padova), 35137 Padova, Italy*

[b]*Dipartimento di Matematica Pura ed Applicata, Via Belzoni 7, 35131 Padova, Italy*

[c]*Istituto Nazionale per la Fisica della Materia, Unita' di Milano, Dipartimento di Fisica, Università di Milano, Via Celoria 16, 20133 Milano, Italy*

Received 17 February 1998; accepted 23 November 1999

Abstract

The flow perturbation around a circular rigid particle during simple shear deformation has been investigated for both Newtonian and non-Newtonian (power-law) fluids by finite-element modelling. If the particle is rotating under the applied shear couple and no-slip occurs at the particle–fluid interface, a 'bow-tie-shaped' streamline pattern results for both Newtonian and power-law fluids and the shape of streamlines does not change noticeably if the stress exponent (n) is changed. In contrast, if the fluid is allowed to separate from the particle, a 'double-bulge-shaped' flow develops in the case of Newtonian fluids, and the type of streamline pattern is influenced by n. We suggest that both stair-stepping and non-stair-stepping geometries of porphyroclast tails may be produced in mylonites, depending on the degree of coherence between the porphyroclasts and the embedding matrix. A different behaviour of the fluid–particle interface may occur as the result of changing fluid rheology, owing to the contrasting stress fields developed for Newtonian and non-Newtonian fluids.

1. Introduction

Porphyroclasts and porphyroclast systems in mylonites have been a subject of increasing attention in recent years (Passchier and Simpson, 1986). Firstly, fabric asymmetry around porphyroclasts is a reliable indicator of the sense of shear and may be used in tectonic reconstructions (e.g. Mawer, 1987; Pennacchioni and Guermani, 1993). Secondly, elliptical porphyroclasts exceeding a critical axial ratio rotate towards equilibrium (sink) positions in general non-coaxial deformation ($0 < W_k < 1$, where W_k is the kinematic vorticity number; Passchier, 1987). The angle between the shear plane and the major axis of a porphyroclast at rest is a function, for a given aspect ratio, of the bulk vorticity (Passchier, 1987; Masuda et al., 1995) and may be used to infer the regime of natural deformation. Lastly, the geometry of porphyroclast systems may store information on the rheological properties of the embedding matrix and allow inference on the type of flow occurring in the lithosphere. On the basis of experimental deformation of rock analogues in an annular shear zone apparatus, it has been suggested that either a non-stair-stepping or stair-stepping geometry of porphyroclast wings (Fig. 1a, b) develops in the case of either Newtonian or power-law (non-Newtonian) creep of the matrix, respectively (Passchier and Sokoutis, 1993; Passchier et al., 1993). The different porphyroclast geometries have been related to the contrasting type of matrix flow developing in the two cases, which is characterized by an eye-shaped or bow-tie-shaped separatrix (Fig. 1c, d) (ten Brink and Passchier, 1995; Passchier, 1993, 1994; Passchier and Sokoutis, 1993).

The possibility of getting information on the type of

* Corresponding author.
E-mail address: pengio@epidote.dmp.unipd.it (G. Pennacchioni).

0191-8141/00/$ - see front matter
PII: S0191-8141(99)00180-7

constitutive equations using porphyroclast geometry has important implications. The knowledge of the actual rheology of rocks during ductile flow at depth is important for models of seismic character of the lithosphere and of large scale geodynamic processes, as well as for understanding the actual mechanisms operating in rocks at high homologous temperatures. The analysis of porphyroclast geometry has important advantages for determining rock rheology: data can be collected by simple optical analysis or directly on hand specimens, porphyroclast geometry is rather insensitive to annealing processes, and the geometry is clearly related to the bulk flow of the embedding matrix.

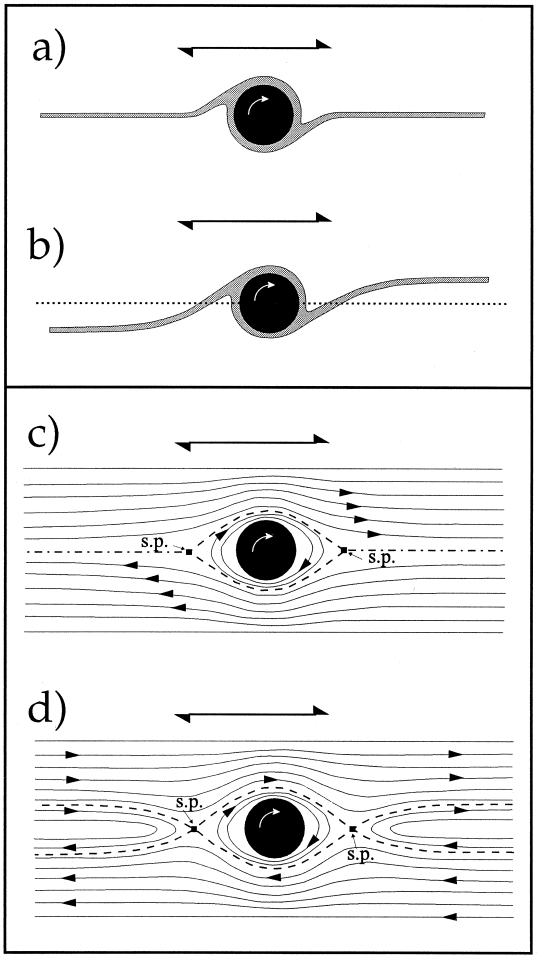

Fig. 1. (a, b) Topology of δ-shaped porphyroclast systems: porphyroclasts (black) without stair-stepping recrystallization wings (a) and with stair-stepping geometries (b). In stair-stepping topologies the porphyroclast wings are not in-plane, i.e. they do not lie, far away from the porphyroclast, on the marker plane parallel to the shear plane passing through the centre of the porphyroclast (dotted line in b). (c, d) Types of streamline patterns described in viscous flow past a sphere during simple shear far-field deformation. Flows are characterized by an eye-shaped separatrix (c) or by a bow-tie-shaped separatrix (d). The separatrix is the dashed line that separates open from closed streamlines; stagnation points (s.p.) and stagnation lines (dots and dashes) are immobile 'regions' of the fluid.

However, this first requires that the variation of porphyroclast geometry can be unequivocally related to matrix rheology, and this is not yet fully established.

Experimental data on rock analogue material (Passchier and Sokoutis, 1993; Passchier, 1993, 1994; ten Brink and Passchier, 1995) are not identical with the numerical results of Masuda and Mizuno (1996a, b). Based on finite-element modelling, these authors report 'double-bulge-shaped' streamline patterns (similar to a flow with an eye-shaped separatrix, but where the separatrix makes a tangent at infinity to the shear plane) with stress exponents (n) ranging from 1 (Newtonian flow) to 5 (power-law flow). Therefore, according to Masuda and Mizuno (1996a), porphyroclast system geometry cannot be used as a gauge for the stress sensitivity of the strain rate. The numerical analysis and experiments only agree in predicting a similar type of flow in Newtonian fluids and these results are also in accordance with the available theoretical analyses (Cox et al., 1968; Masuda and Ando, 1988; Gray and Busa, 1994; Bjørnerud and Zhang, 1995).

This paper is an attempt to explain, using numerical modelling, the different flow patterns obtained experimentally in viscous fluids and, therefore, of the different porphyroclast geometries. In a simple model for a porphyroclast, we aim to show that, if a rigid spherical object is set in a fluid undergoing simple shear, the combined effect of differences in the coherence at the fluid–particle interface and the fluid rheology may control the transition from one type of flow to another.

2. Theoretical background

Incompressible viscous fluid rheology is widely accepted as a good approximation for rock behaviour undergoing ductile deformation at relatively high homologous temperatures. The constitutive equation for viscous fluids may be expressed as

$$\tau_{ij} = \mu d_{ij} \tag{1}$$

where μ is the viscosity, τ_{ij} is the deviatoric stress tensor and d_{ij} is the shear-rate tensor. A fluid is called Newtonian if, for a given temperature, the viscosity is a constant, otherwise non-Newtonian. For non-Newtonian fluids the viscosity is supposed to follow a power-law equation

$$\mu = \mu_0 D^{1/n-1} \tag{2}$$

where

$$D = \left(\frac{1}{2} \sum_{i,j=1}^{3} d_{ij} d_{ij} \right)^{1/2}$$

μ_0 is a constant and n (also known as stress exponent) is a phenomenological parameter, such that the fluid is Newtonian if $n = 1$.

The dynamics of a viscous fluid obeys complex non-linear partial differential equations that strongly depend on the stress tensor properties (e.g. Malvern, 1969). In general, these equations can be solved only by heavy numerical computations (e.g. Zienkiewicz and Taylor, 1994). For the steady-state motion of a viscous, incompressible Newtonian fluid at low Reynolds number, the dynamical equations reduce to the simplified Navier–Stokes equations

$$\mu\nabla^2\mathbf{u} = \nabla p \quad \text{and} \quad \nabla\cdot\mathbf{u} = 0 \tag{3}$$

where μ is the viscosity, $\mathbf{u} = (u_1, u_2, u_3)$ is the velocity vector and p is the pressure. Analytical solutions of the above equations are available in some simple cases (e.g. Lamb, 1932).

In most mylonites, porphyroclast shape closely approaches a sphere or an ellipsoid and matrix flow is highly non-coaxial. The spherical and ellipsoidal porphyroclast shapes are the result of grain refinement processes during porphyroclast rotation, which tend to eliminate sites of high stress concentration (ten Brink and Passchier, 1995). The component of non-coaxiality of the mylonitic flow can be inferred from the asymmetry of mylonitic textures (e.g. Passchier and Trouw, 1996). Therefore, the simplest model of a porphyroclast in a mylonite is a rigid sphere embedded in a viscous fluid deformed by simple shear.

In the case of the flow of a Newtonian fluid past a rotating sphere during simple shear far-field deformation, analytical solutions have been suggested by a few authors (Cox et al., 1968; Masuda and Ando, 1988; Gray and Busa, 1994; Bjørnerud and Zhang, 1995). However, a careful overview of the literature establishes the difficulties involved in trying to solve Eq. (3) analytically (for the boundary conditions under consideration) and, to our knowledge, no exact solution is currently available.

Cox et al. (1968) calculated the velocity field past a rotating cylinder during simple shear deformation and also provide a formula for the velocity field past a sphere. However a direct substitution shows that the suggested formula is not an exact solution of Eq. (3).

Masuda and Ando (1988) derived an approximate expression of the velocity components of simple shear flow past a rotating sphere by summing two 'elementary' velocity fields: (i) the velocity u^{a} of a general viscous flow around an immobile rigid sphere, and (ii) the velocity u^{b} induced by a rotating sphere in an immobile (at infinity) fluid. u^{a} is written as a linear composition of solid spherical harmonics including arbitrary terms up to degree 2 to get an approximate solution. u^{b} is the exact solution of Lamb (1932, pp. 588–589).

Bjørnerud and Zhang (1995) adopted an approach similar to that of Masuda and Ando (1988) and calculated the velocity field by summing the two exact analytical solutions of Lamb (1932) for the above cases (i) and (ii). In the case (i), the analytical solution of Lamb (1932, pp. 588–589) is expressed as a function of the parameter U [which is the velocity component u_1 at infinity where the boundary conditions are $\mathbf{u}^{\mathrm{a}} = (U, 0, 0)$]. Bjørnerud and Zhang (1995) have used the Lamb's (1932) solution to obtain the simple shear flow past an immobile sphere by substituting the quantity U with $U = U(x_2) = U_0 x_2/h$, where U_0 is a constant and h is the half-width of the shear zone. However, this substitution is not allowed because U is a constant in Lamb's original solution, not a variable that may vary with x_i.

According to Gray and Busa (1994), if a generic far-field spatial-gradients-of-the-velocity tensor $L_{ij} = \partial u_i/\partial x_j$ is known, the velocity field around a sphere may be calculated with a formula that is a generalization of the one calculated, in the case of a pure shear deformation around an immobile sphere, by Einstein (1956). However the proposed formula does not tend to apply to any generic tensor L_{ij} (for example the case of a far-field translation or rotation).

Because of these difficulties related to the analytical solution of the problem (and, it should be noted, no theoretical analysis is available at all for non-Newtonian fluids), a numerical approach to the problem was employed.

3. Finite element model

We have analyzed the geometry of the flow past a rotating sphere by the Finite Element Method (FEM) (e.g. Zienkiewicz and Taylor, 1994) for the case of a viscous fluid with different rheologies (from Newtonian to strongly non-Newtonian) undergoing simple shear far-field deformation. For simplicity, we have initially performed a detailed 2D analysis (equivalent to the analysis of a section through an infinitely long cylinder), which is in agreement qualitatively with preliminary 3D results. To exclude the possibility that some code-dependent effects may have occurred, we have used two different FEM codes. Moreover, the 'reliability' of the numerical results has been previously checked by reproducing some simple cases for which exact analytical solutions are known (e.g. Lamb, 1932).

3.1. 2D model

3.1.1. Model geometry

The geometric model for our analysis is shown in Fig. 2(a). The model takes into account only a quarter

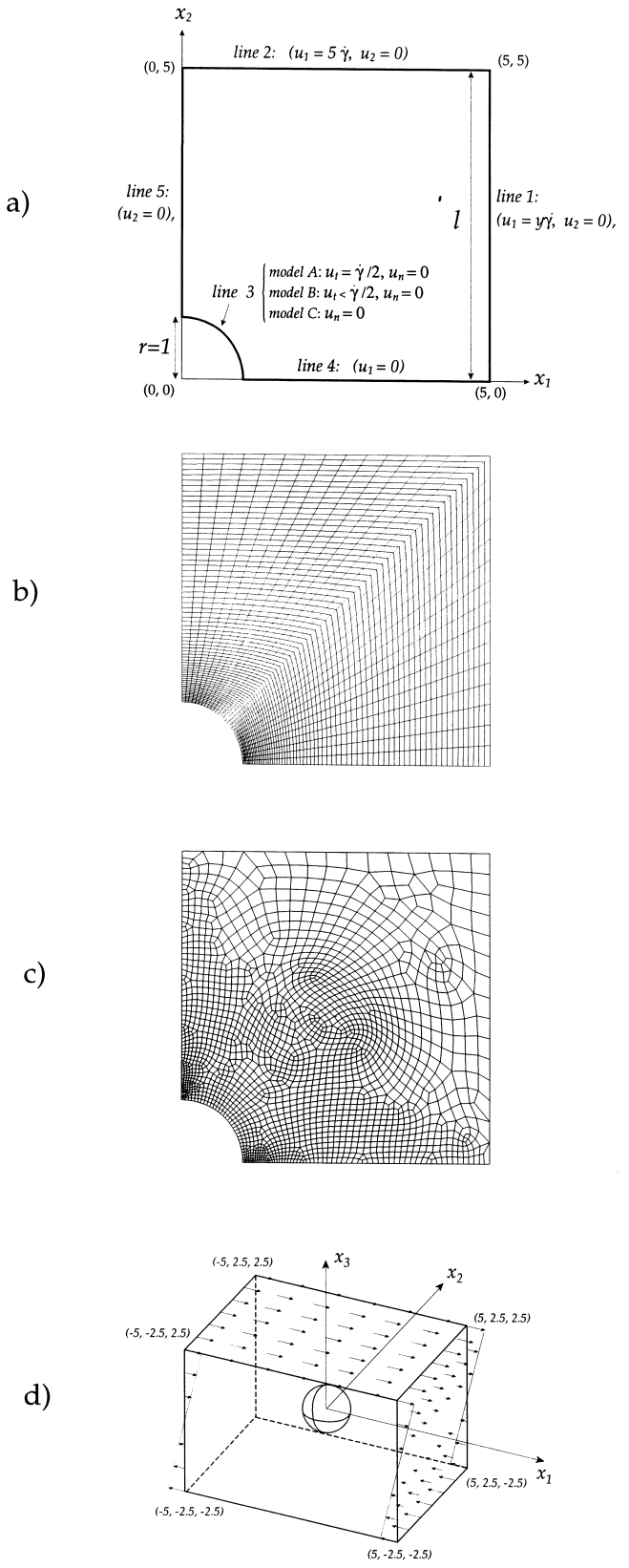

Fig. 2. (a) Geometric model for the FEM analysis ($l = 5$) and boundary conditions. (b) Four-node quadrilateral mesh mainly used in this study. (c) Automatically generated paved mesh. (d) 3D model.

of the structure, reflecting the symmetry of the analysis. The origin of the Cartesian coordinate system x_1–x_2 is placed at the centre of the particle and the particle radius (r) is set to 1. In order to evaluate the influence of the model size we studied different cases by changing ratio between the size (l) of the analyzed square area and the particle radius ($r = 1$). Values of l in the range of 2.68 (as in Masuda and Mizuno's model) to 25 have been investigated (Fig. 2a reports the model with $l = 5$). We expected that, since boundary conditions on line 1 and line 2 simulate a far-field simple shear deformation, the model must have a minimum size below which the results are conditioned by the size of the model.

3.1.2. Mesh

The mesh for $l = 5$ includes 2204 quadrilateral elements and 2108 nodes (Fig. 2b). Considering the fact that flow perturbation will appear around the sphere, we refined the mesh close to the particle. Models with $l > 2.68$, have been built by adding elements to the same $l = 2.68$ mesh. In some models, the mesh type has been varied to establish if it has any significant influence on the results. In these cases, we used either a mesh internally generated by the program (paved mesh: Fig. 2c) or have re-meshed with a high-resolution grid.

3.1.3. Boundary conditions (Fig. 2a)

The far-field, steady-state, clockwise simple shear deformation is simulated by assigning velocity components

$$u_1 = \dot{\gamma} x_2 \quad \text{and} \quad u_2 = 0 \tag{4}$$

to the nodes of line 1 and line 2, where u_1 is the velocity component along the x_1 axis, $\dot{\gamma}$ is the far-field simple-shear strain-rate deformation. Moreover, because of the symmetry of the system, $u_1 = 0$ along the x_1 axis (line 4), and $u_2 = 0$ along the x_2 axis (line 5). A critical point in the numerical modelling is the choice of the boundary conditions on line 3, which represents the fluid at the interface with the rigid particle. Therefore, this point will be discussed in detail. Boundary conditions imposed on velocity in viscous-flow theory usually require that the fluid adhere to any rigid wall (Malvern, 1969). At any stationary wall, the tangential velocity u_t is set to be zero in viscous flow theory, while for an ideal frictionless fluid only the normal component (u_n) is required to vanish at a rigid wall. In the present case, the particle is assumed to rotate in accordance with experience (e.g. Passchier and Sokoutis, 1993). If no slip occurs at the particle–matrix interface, as is assumed in viscous-flow theory, a constant non-zero tangential velocity has to be assigned to the nodes of line 3. In this hypothesis, we

set u_t = constant and $u_n = 0$ on line 3. These boundary conditions were also assumed by Masuda and Mizuno (1996a) in their models. The magnitude of the tangential velocity is set to be half the simple shear rate of the far-field deformation ($\dot{\gamma}$) in both Newtonian and non-Newtonian matrix flow, in accordance with the theory (Jeffery, 1922; Masuda and Mizuno, 1996a): model with these boundary conditions is referred to as Model A.

The above boundary conditions along line 3, are consistent with the behaviour of an ideal viscous fluid. However, experimental results (e.g. Ildefonse and Mancktelow, 1993) and observation in mylonites indicate that detachment may occur to some degree at the fluid–particle interface. Detachment has been modelled by some authors by reducing the angular velocity of the porphyroclasts (Bjørnerud and Zhang, 1995) in accordance with experiments that indicate relatively small rotation rates compared to theoretically expected ones (Passchier and Sokoutis, 1993). We have investigated in Model B the effects of reducing the rotation velocity of porphyroclasts on flow lines by assigning a constant tangential velocity $u_t < \dot{\gamma}/2$ to the nodes of line 3. However, the boundary conditions in Model B do not actually represent detachment of the fluid from the particle since, if a loss of interface coherence occurs somewhere, the tangential velocity cannot be set at a constant value along the whole particle surface. As an end member situation, opposite to the case where fluid is completely adhered to the particle wall, we have considered the case of a completely detached surface (Model C). In Model C only the normal component of velocity is fixed along line 3 ($u_n = 0$), while the tangential velocity is unconstrained. This is probably not the case in most real situations and experiments with viscous fluids in which detachment occurs on 'discrete' fluid–particle interface segments where the resolved shear stress exceeds a critical value.

3.1.4. Input data

Newtonian to strongly non-Newtonian power-law rheology of the fluid has been considered by varying the stress exponent from 1 to 10. In fact, the dominant deformation mechanism in many crystalline materials has been shown to change from power-law dislocation creep, with n normally in the range of 3–5 (Kirby, 1985), to diffusional creep or Harper–Dorn Newtonian dislocation creep (Wang et al., 1994), for which n approaches 1 (Newtonian viscous). In addition, superplasticity, thought to be a main deformation mechanism in many fine-grained mylonites, is characterized by power-law constitutive equation with $n = 1$–2.5, and some experimental rock deformation studies have reported stress exponents as high as 11 (Kirby and McCormick, 1984).

We have modelled deformation under both geological and experimental conditions. For the geological deformation we used strain rate values in the range of 10^{-14}–10^{-12} s^{-1}, viscosities in the range of 10^{19}–10^{23} kg m^{-1} s^{-1} and a density of 2.7×10^3 kg m^{-3}, which correspond to very low Reynolds numbers (1.35×10^{-30}–1.35×10^{-36}). For laboratory deformation we used data from the experimental runs and materials (polydimethyl-siloxano: PDMS) of Passchier and Sokoutis (1993): strain rate = 10^{-3}–10^{-1} s^{-1}; viscosity = 5×10^4 kg m^{-1} s^{-1}; density = 9.65×10^2 kg m^{-3} (for material parameters see Weijermars, 1986). Reynolds numbers are in the range of 9.65×10^{-9}–10^{-7}.

Because of the very large differences in the order of magnitude of the terms involved in the equations (compare viscosities with strain rate values), a dimensionless formulation of the problem has been used, to reduce the possible ill-conditioning of the matrices involved in the calculations. In dimensionless formulation the quantities, u_i and x_i, and time t are scaled with respect to a characteristic speed S and a characteristic length Λ. The dimensionless velocities u_i^* and distances x_i^* are defined by the relations $u_i^* = u_i/S$, and $x_i^* = x_i/\Lambda$. In the case of simple shear flow in a Newtonian incompressible fluid, the system of equations of momentum conservation may be written as

$$\mathrm{Re}\sum_{j=1}^{3} u_j^* \frac{\partial u_i^*}{\partial u_j} = -\frac{\partial p^*}{\partial x_i} + \sum_{j=1}^{3} \frac{\partial d_{ij}^*}{\partial x_j} \tag{5}$$

where $\mathrm{Re} = \rho S \Lambda/\mu$ (Re: Reynolds number), $p^* = p\Lambda/\mu S$, $d_{ij}^* = d_{ij}(\Lambda/\mu S)$. This representation of the momentum equation is a good choice for low Reynolds numbers. However, there is not a unique representation of the momentum equation. A simple rearrangement of the above equation results in

$$\sum_{j=1}^{3} u_j^* \frac{\partial u_i^*}{\partial u_j} = -\frac{\partial p^{**}}{\partial x_i} + \frac{1}{\mathrm{Re}} \sum_{j=1}^{3} \frac{\partial d_{ij}^*}{\partial x_j} \tag{6}$$

where $p^{**} = p/(\rho S^2)$. This second set of equations is more appropriate for high Reynolds numbers.

3.2. 3D model

Consider the 3D geometry shown in Fig. 2(d), where a sphere is present in a fluid undergoing simple shear (the plane x_1–x_2 is the shear plane and x_1 is the shear direction). In contrast to the case of a cylinder, the flow around a sphere will include u_2 velocity components. Therefore, the streamline pattern obtained in 2D models cannot be uncritically assumed to be a good model for the flow around a sphere. We have run some 3D tests with boundary conditions consistent with those of 2D models as illustrated in

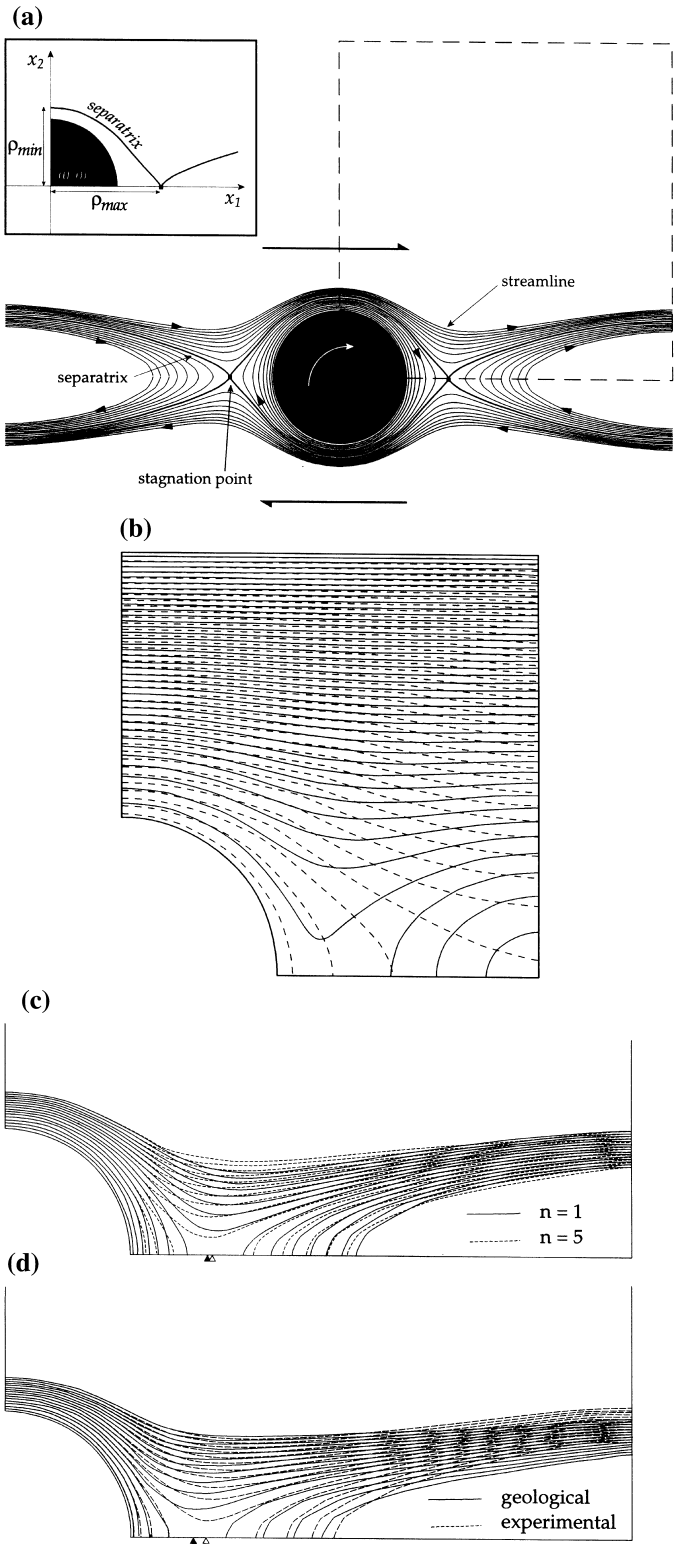

Fig. 3. (a) Bow-tie-shaped perturbation of streamlines around a circular particle in clockwise simple shear flow. The dashed line represents the FEM analysis area. In the upper left-corner inset, the meaning of ρ_{max} and ρ_{min} is shown. (b) Contrasting streamline patterns obtained for Newtonian fluids with different nondimensionalization equations: the solid and dashed lines indicate streamlines obtained with Eq. (2a) and (2b), respectively. (c) Influence of n on streamline patterns; the open and filled triangles indicate the position of ρ_{max} in the case of $n = 1$ and $n = 5$, respectively. (d) Comparison between FEM models of geological and experimental deformations in the case of $n = 10$; the open and filled triangles indicate the position of ρ_{max} in the case of the geological and experimental simulation, respectively.

Fig. 2(d). The results are only briefly summarized here, and a complete 3D is still in progress and will be presented elsewhere.

4. Results and discussion

Unless otherwise stated, we only present the results for models with size $l = 5$ (Fig. 2a) calculated with a mesh as in Fig. 2(b). The results can be summarized as follows.

4.1. Model A: constant tangential velocity of the fluid at the particle interface ($u_t = \dot{\gamma}/2$)

The streamline patterns are always bow-tie-shaped (Fig. 3a), irrespective of the value of the stress exponent in the range of $1 < n < 10$. A bow-tie-shaped streamline pattern is characterized by three separatrices which end on two 'hyperbolic stagnation points' (that are immobile in the flow) on both sides of the central object. This type of streamline pattern has been obtained in experiments by tracing the path lines of marker particles in a fluid close to porphyroclasts (ten Brink and Passchier, 1995) and is consistent with a flow pattern suggested by Ottino (1989). Our numerical results are in part contradictory to the inferences of Passchier et al. (1993), who suggested that a bow-tie-shaped separatrix only develops in the case of $n > 1$. This was the basis of their suggestion that stair-stepping and non-stair-stepping geometries may be used to distinguish between a non-Newtonian and Newtonian matrix rheology. The fact that the type of streamline pattern remains unchanged for $n = 1$ and $n > 1$ flows was the main conclusion of Masuda and Mizuno (1996a), but they obtained a double-bulge-shaped particle path in their FEM model. The reason for this difference is difficult to determine in the absence of more specific details about their model. However, we succeeded in reproducing the same streamline pattern as in Masuda and Mizuno under the same boundary conditions by changing the nondimensionalization equation. If Eq. (6) is used instead of Eq. (5), the streamline pattern changes from bow-tie to apparently double-bulge-shaped. The two different streamline patterns obtained with the two different nondimensionalizations are drawn in Fig. 3(b). However, Eq. (6) should only be used in the case of high Reynolds numbers when inertial effects are dominant over viscous effects, which is not the case for deformation considered.

The influence of the n value on the results is negligible, at least in the range $n = 1$–5. A streamline pattern can be characterized by the distances from the origin, measured on the x_1 and x_2 axis, of the most distant closed particle path around the circular porphyroclast. The two values, representing the farthest and the nearest points of the particle path, are referred to as ρ_{max} and ρ_{min}, respectively (Cox et al., 1968; Masuda and Mizuno, 1996a) (see inset of Fig. 3a). In our model, changing n produces only very minor variations in the ρ_{max} and ρ_{min} values (Fig. 4) and of the particle paths (Fig. 3c). In any case, these minor differences are unlikely to produce contrasting porphyroclast morphologies useful for discriminating the rheological properties of the matrix in mylonites.

The results of the simulations using experimental parameters are very similar to those discussed above for geological deformation, despite the very large difference in the Reynolds number (up to 29 orders of magnitude). In the case of Newtonian flow, the calculated streamline patterns for experimental and natural deformation are practically indistinguishable from each other, whereas some differences may be discerned at high n values (Figs. 3d and 4). However, the values ρ_{max} and ρ_{min} for geological and experimental conditions are quite similar even in the case of strongly non-Newtonian fluid. This fact justifies the use of analogue scale models to simulate natural deformation.

The results of the FEM analysis are strongly conditioned by the size l of the model. This is well illustrated by the change of ρ_{max} and ρ_{min} with changing l (Fig. 5). The value of ρ_{max} significantly increases with increasing l. In addition, ρ_{max} is largely uninfluenced by the n value in the range of l between 5 and 12, but shows a strong dependence on n, as well as on l, for $l > 15$ and $l < 5$. The value of ρ_{min} is relatively uninfluenced by l and n for models with $l < 12$; for $l > 12$,

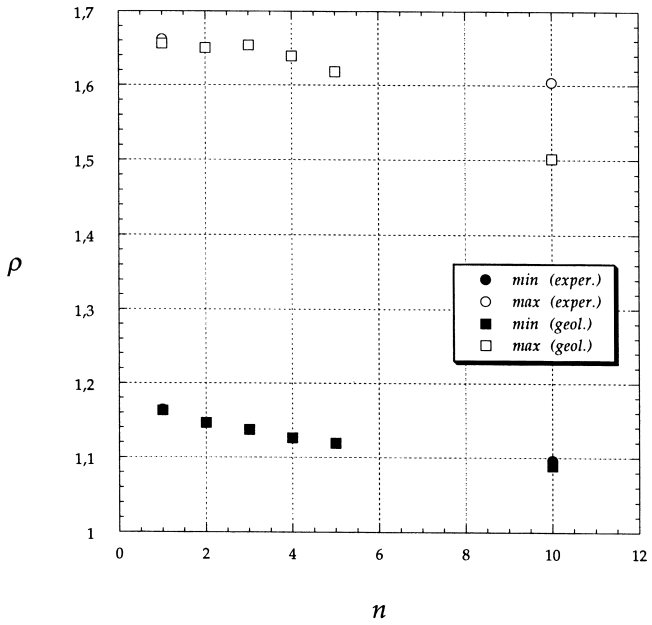

Fig. 4. Dependence of ρ_{max} and ρ_{min} on n, in an $l = 5$ model with no-slip conditions at the particle–fluid interface (Model A).

ρ_{min} remains nearly constant with changing l in Newtonian fluids, but shows a strong dependence on l in non-Newtonian fluids. A similar mismatching between ρ_{max} values at different n also results in the case of $l = 2.68$. However, we consider this model inadequate since the boundary conditions at line 1 and line 2 hardly simulate in this case a far-field deformation because of the small size of the model.

Because of the way the different meshes were built, namely by adding elements to the same $l = 2.68$ mesh, comparing models with different l also means comparing results calculated with different meshes. Some dependence of r on l may therefore be simply related to these mesh differences. Moreover, this way of building the mesh results in strongly elongate elements toward line 1 and line 2 at large l, which may introduce numerical problems and at least in part explain the dependence of r on l. To test the possible influence of varying the mesh on results, we also performed some models with a paved mesh, automatically generated by the program and an additional high-resolution mesh. The test results demonstrate that the influence of the mesh is negligible.

4.2. Model B: 'reduced' tangential velocity of the fluid at the particle interface ($u_t < \dot{\gamma}/2$)

The streamline pattern still develops the same bow-tie shape for both Newtonian and non-Newtonian fluids as in the previous Model A examples. Decreasing the tangential velocity from half the bulk shear strain rate at the particle–fluid interface causes the outermost closed particle path to shrink around the porphyroclast. This is in accordance with the results of Bjørnerud and Zhang (1995). The effect of decreasing u_t on ρ_{max} and ρ_{min} values is shown in the plot of Fig. 6.

4.3. Model C: unconstrained tangential velocity of the fluid at the particle interface

In contrast to the results for Model A and B, when slip is allowed at the particle–fluid interface the streamline pattern is strongly dependent on the fluid rheology and, in particular, contrasted flow geometries are obtained for Newtonian and non-Newtonian fluids. In the case of Newtonian fluids, the flow is characterized by a double-bulge-shaped separatrix topology (Fig. 7a), which is consistent in this case with the experimental results of Passchier and Sokoutis (1993). Non-Newtonian fluids are instead characterized by the flow type reported in Fig. 7(b), which is quite different from the previously described flow categories (Fig. 1c, d). With respect to both eye and bow-tie-shaped streamline patterns, this flow does not include closed particle paths around the sphere and the separatrix effectively abuts against the porphyroclast. This type of pattern already appears at $n = 2$.

As in Model A, a strong dependence of streamlines on the model dimension (l) is found. For any given n, the streamline patterns calculated for different l are of the same type, but are not coincident. As in the previous models, there is a negligible influence of the mesh and input parameters (i.e. 'geological' or 'experimental') on the results.

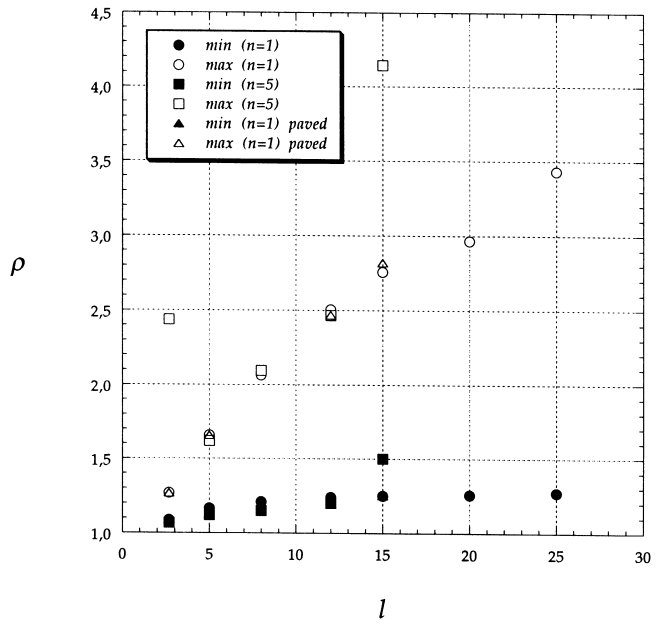

Fig. 5. Dependence of ρ_{max} and ρ_{min} on the model size (l) in Model A.

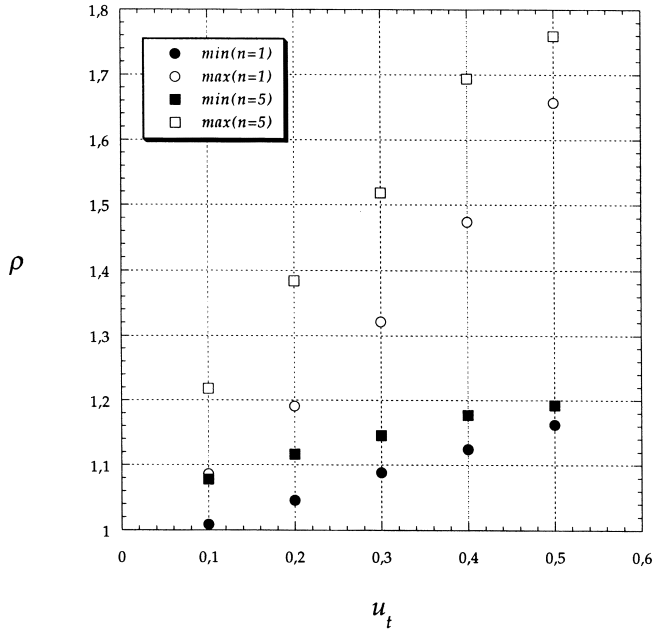

Fig. 6. Dependence of ρ_{max} and ρ_{min} on the values of the tangential velocity u_t imposed at the particle–boundary interface (Model B).

4.4. 3D models

3D analysis implies severe numerical computation and a high hardware performance is required for a detailed study. We anticipate here only preliminary results, but we stress that a more refined analysis is necessary to allow a more definitive interpretation. On the plane x_1–x_3 of the 3D model (i.e. the plane through the centre of the sphere, normal to the shear plane and containing the shear direction) the following qualitative observation can be made:

(a) In Model A, independent of the value of n in the range $1 < n < 5$, the particle paths include parabolic trajectories around the x_1 axis at a certain distance from the rigid sphere consistent with 2D flow types characterized by a bow-tie-shaped separatrix. This legitimizes the use of 2D models to obtain information on the type of streamline pattern around a sphere.

(b) The streamline patterns calculated in the 3D analysis are characterized by a noticeable shrinking of closed particle paths with respect to those calculated in 2D models. This effect was already reported by Cox et al. (1968) as a main difference between the flow patterns around a cylinder and a sphere. This indicates that the amount of stair-stepping calculated in 2D models overestimates the one occurring around a sphere and this may have some influence in interpretation of porphyroclast system geometry as a rheological gauge.

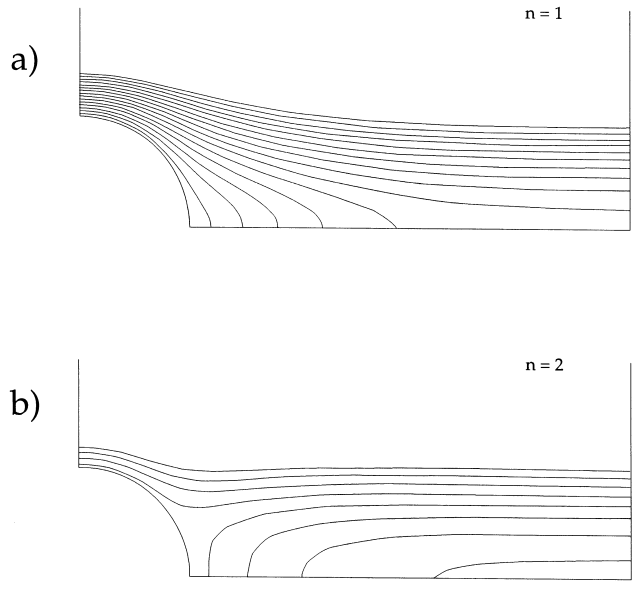

Fig. 7. Streamline patterns obtained in Newtonian (a) and non-Newtonian fluids (b) when complete detachment occurs at the particle–fluid interface (Model C).

5. Conclusions

FEM investigation of the distortion of simple shear viscous flow around a rigid sphere has produced several important results that can be used in the interpretation of porphyroclast systems in mylonites and analogue scale-model experiments. We were able to reproduce both the streamline patterns observed experimentally (Passchier and Sokoutis, 1993; Passchier, 1993, 1994; ten Brink and Passchier, 1995), but the change in the flow pattern from types characterized by an eye-shaped separatrix to ones with a bow-tie-shaped one does not occur simply as the result of changing the fluid rheology, as suggested by these authors, but was only possible by changing the boundary conditions.

An important result of our FEM models is that the difference in the flow patterns found in experiments is probably related to a difference in the degree of coherence of the fluid–particle interface. Although particle–matrix decoupling is not generally considered in viscous fluid theory, it commonly occurs in natural cases, as demonstrated by observations in natural mylonites (where pressure shadows around porphyroclasts are common) and by experiments with rock analogues (Ildefonse and Mancktelow, 1993). In our FEM models, a no-slip condition between fluid and porphyroclast always produces only one type of flow independent on the fluid rheology, whether Newtonian or power-law (with $1 < n < 10$). The fluid flow is characterized by a bow-tie-shaped separatrix. As a consequence, δ-shaped porphyroclast systems in mylonites will show stair-stepping geometries of recrystallized wings if the matrix is coherent with the embedded porphyroclasts. In the case of a coherent particle–fluid interface the influence of the fluid rheology on streamline-patterns is negligible and, therefore, no differences in morphology of stair-stepping porphyroclast systems that could be used to infer the matrix rheology (and in particular n values) in mylonites are expected to occur.

In Newtonian fluids, the development of streamline patterns with a double-bulge shape is possible when detachment occurs at the fluid–particle interface. Therefore, non-stair-stepping recrystallization wings are effectively related to linear viscous rheology of the matrix in mylonites (as suggested on the basis of experimental work), but only if decoupling of the matrix occurs around porphyroclasts. When detachment occurs, the streamline-pattern type is conditioned by the rheology of the fluid and, in non-Newtonian fluid, the flow calculated numerically could be consistent with σ-type porphyroclast geometries.

Our study is limited to the numerical analysis of two end-member cases, i.e. perfect coherence or complete detachment of the fluid–particle interface, under different fluid rheologies. In both experiments and mylonites, this will not be the case. When detachment

occurs, it probably affects only discrete portions of the particle surface where the shear stress exceeds a critical frictional value. Therefore, the real distribution of detachment reflects the heterogeneous stress distribution around a porphyroclast as well as the 'roughness' characteristic of the particle surface. A more detailed study of detachment is needed. However, our analysis indicates that caution must be used when attempting to use porphyroclast geometry in mylonites to infer the rheology of the matrix, since the streamline patterns are a complex function of the rheology of the fluid and of the degree of coherence between fluid and particle. This is in accordance with the observations of Bjørnerud and Zang (1995).

If analyzed in the light of the present results, the experimental data of Passchier and Sokoutis (1993) and ten Brink and Passchier (1995) may indicate that detachment is not equally likely to occur in Newtonian and non-Newtonian fluids. This is a reasonable consequence of the change in the stress fields associated with changing n, and therefore the same boundary conditions may not be appropriate for different fluid rheologies. It would be important to verify this hypothesis experimentally by monitoring in detail the relative velocity of the fluid close to the particle interface. Combined experimental and numerical studies together with detailed observations on natural mylonites are necessary to better understand the behaviour of porphyroclast systems, since they still have a great potential for placing constraints on the rheology of rocks in the domain of ductile deformation.

Acknowledgements

We greatly acknowledge N. Mancktelow, G. Ranalli and an anonymous reviewer for review. This work was supported by grants from M.U.R.S.T (G.V. Dal Piaz and M. Morandi-Cecchi).

References

Bjørnerud, M.G., Zhang, H., 1995. Flow mixing, object–matrix coherence, mantle growth and the development of porphyroclasts tails. Journal of Structural Geology 17, 1347–1350.

Cox, R.G., Zia, Y.Z., Mason, S.G., 1968. Particle motion in sheared suspensions. XXV. Streamline around cylinders and spheres. Journal of Colloid and Interface Science 27, 7–18.

Einstein, A., 1956. Investigation on the Theory of the Brownian Movement. Dover, New York.

Gray, N.H., Busa, M.D., 1994. The three-dimensional geometry of simulated porphyroblast inclusion trails: inert-marker, viscous flow model. Journal of Metamorphic Geology 12, 575–597.

Kirby, S.H., 1985. Rock mechanics observations pertinent to the rheology of the continental lithosphere and the localisation of strain along shear zones. Tectonophysics 119, 1–27.

Kirby, S.H., McCormick, J., 1984. Inelastic properties of rocks and minerals: strength and rheology. In: Carmichael, R.S. (Ed.), Handbook of Physical Properties of Rocks, vol. iii. CRC Press, Boca Raton, FL, pp. 140–280.

Ildefonse, B., Mancktelow, N., 1993. Deformation around rigid particles: the influence of slip at the particle matrix interface. Tectonophysics 221, 345–359.

Jeffery, G.B., 1922. The motion of ellipsoidal particles immersed in a viscous fluid. Proceedings of the Royal Society of London, Series A 102, 161–179.

Lamb, H., 1932. Hydrodynamics. Cambridge University Press, Cambridge.

Malvern, L.E., 1969. Introduction to the Mechanics of a Continuum Medium. Prentice-Hall, Englewood Cliffs, NJ 713 pp.

Masuda, T., Ando, S., 1988. Viscous flow around a rigid spherical body: a hydrodynamical approach. Tectonophysics 148, 337–346.

Masuda, T., Michibayashi, K., Otha, H., 1995. Shape preferred orientation of rigid particles in a viscous matrix: re-evaluation to determine kinematic parameters of ductile deformation. Journal of Structural Geology 17, 115–129.

Masuda, T., Mizuno, N., 1996a. Deflection of non-Newtonian simple shear flow around a rigid cylindrical body by the Finite Element Method. Journal of Structural Geology 18, 1089–1100.

Masuda, T., Mizuno, N., 1996b. Computer modelling of mantled porphyroclasts in Newtonian and non-Newtonian simple shear viscous flow. Journal of Structural Geology 18, 1487–1491.

Mawer, C.K., 1987. Shear criteria in the Grenville Province, Ontario, Canada. Journal of Structural Geology 9, 531–539.

Ottino, J.M., 1989. The Kinematics of Mixing Stretching, Chaos and Transport. Cambridge University Press, Cambridge.

Passchier, C.W., 1987. Stable positions of rigid objects in non-coaxial flow—a study in vorticity analysis. Journal of Structural Geology 9, 679–690.

Passchier, C.W., 1993. Experimental modelling of mantled porphyroclasts. Journal of Structural Geology 15, 895–909.

Passchier, C.W., 1994. Mixing in flow perturbations: a model for development of mantled porphyroclasts in mylonites. Journal of Structural Geology 16, 733–736.

Passchier, C.W., Simpson, C., 1986. Porphyroclasts systems as kinematic indicators. Journal of Structural Geology 8, 831–843.

Passchier, C.W., Sokoutis, D., 1993. Experimental modelling of mantled porphyroclasts. Journal of Structural Geology 15, 895–909.

Passchier, C.W., ten Brink, C.E., Bons, P.D., Sokoutis, D., 1993. δ objects as a gauge for stress sensitivity of strain rate in mylonites. Earth and Planetary Science Letters 120, 239–245.

Passchier, C.W., Trouw, R.A.J., 1996. Microtectonics. Springer-Verlag, Berlin.

Pennacchioni, G., Guermani, A., 1993. The mylonites of the Austroalpine Dent Blanche nappe along the northwestern side of the Valpelline valley (Italian Western Alps). Memorie di Scienze Geologiche 45, 37–55.

ten Brink, C.E., Passchier, C.W., 1995. Modelling of mantled porphyroclasts using non-Newtonian rock analogue materials. Journal of Structural Geology 17, 131–146.

Wang, J.N., Hobbs, B.E., Ord, A., Shimamoto, T., Toriumi, M., 1994. Newtonian dislocation creep in quartzites: implications for the rheology of the lower crust. Science N.Y. 265, 1204–1206.

Weijermars, R., 1986. Flow behaviour and physical chemistry of bouncing putties and related polymers in view of tectonic laboratory applications. Tectonophysics 124, 325–358.

Zienkiewicz, O.C., Taylor, R.L., 1994. The Finite Element Method. Volume 1: Basic Formulation and Linear Problems. McGraw-Hill, London.